University of Crete & Skinakas Observatory

Department of Physics

Thesis for the degree of

Bachelor of Science on Physics

Spectroscopic study of the Be optical counterpart to the high-mass X-ray binary source IGR J21343+4738

Psaradaki Ioanna

Supervisors: Prof. Andreas Zezas, Dr. Pablo Reig

Heraklion, May 2014

Εισαγωγή

Στόχος της παρούσας διπλωματικής εργασίας είναι η μελέτη των φυσικών ιδιοτήτων του οπτικού συνοδού του διπλού συστήματος αστέρων ακτίνων Χ, IGR J21343+4738. Για το σκοπό αυτό πραγματοποιήθηκε φασματοσκοπική μελέτη του οπτικού αστέρα του συστήματος προκειμένου να εξεταστεί η μεταβλητότητα του στο χρόνο. Χρησιμοποιήθηκαν φασματοσκοπικά δεδομένα από το 2009 έως το 2013 εκ των οποίων τα περισσότερα συγκεντρώθηκαν από το αστεροσκοπείο του Σκίνακα στην Κρήτη. Επιπλέον χρησιμοποιήθηκαν δεδομένα από το τηλεσκόπιο Fred Lawrence Whipple (FLW) στην Αριζόνα και από το William Hershel Telescope (WHT) από το αστεροσκοπείο της La Palma στην Ισπανία.

Από τα φασματοσκοπικά δεδομένα στην κόκκινη περιοχή του οπτικού φάσματος μελετήθηκε η γραμμή Ηα (6563Å) προκειμένου να εξετασθεί η συμπεριφορά του δίσκου που παρατηρήθηκε γύρω από τον οπτικό αστέρα, ενώ από την μπλε περιοχή του φάσματος καθορίστηκε ο φασματικός τύπος του αστέρα και εκτιμήθηκαν η περιστροφική του ταχύτητα και η ακτίνα του δίσκου του.

Από τα δεδομένα προέκυψε ότι ο οπτικός συνοδός του διπλού συστήματος αστέρων ακτίνων Χ IGR J21343+4738 είναι φασματικού τύπου Βe δηλαδή παρουσιάζει γραμμές εκπομπής στο φάσμα του και εμφανίζει επεισόδια απώλειας και επανεμφάνισης του δίσκου του. Παρατηρήθηκε ότι ο δίσκος αυτός εμφανίζεται και εξαφανίζεται με μια περίοδο που διαρκεί τουλάχιστον 4 χρόνια. Επιπλέον από τον υπολογισμό της ταχύτητας περιστροφής του αστέρα συμπεραίνουμε ότι πιθανώς η κύρια αιτία εμφάνισης του δίσκου είναι η γρήγορη περιστροφή του. Τέλος, συγκρίνοντας το βάθος των φασματικών γραμμών του μπλε φάσματος παρουσία του δίσκου και μη, σημειώθηκε ότι οι γραμμές Balmer καθώς και οι γραμμές HeI επηρεάζονται ισχυρά από την ύπαρξη αυτού του δίσκου.

Abstract

The main aspect of this work is to determine the physical properties of the optical counterpart to the INTEGRAL X-ray binary source IGR J21343+4738 and also to study its long-term variability. Spectroscopic data since 2009 in the red region of the optical spectrum allowed to study the Hα line profile (6563Å) in order to determine the variability of the disk and to report a disk loss episode. Additionally, observations in the blue region were used to the spectral classification of the optical star as well as to estimate the rotational velocity of the star and the disk radius.

The Hα line changed from an absorption dominated profile to an emission line profile and then back to absorption. It was found that the optical counterpart to the X-ray source IGR J21343+4738 is a Be star which presents disk-loss episodes with period at least four years. Also the estimation of the rotational velocity of the star showed that the fast rotation of the Be star is the main mechanism that expels matter from the photosphere to create the disk. Finally it was noted that τηε width of the Balmer and HeI lines is strongly affected by the existence of the disc around the Be star.

Acknowledgements

Contents

Chapter1

Introduction

1.1   Binary stars

1.1.1 A brief history of Binary stars

The term *binary* was first used in this context by Sir William Herschel in 1802, when he wrote:

"If, on the contrary, two stars should really be situated very near each other, and at the same time so far insulated as not to be materially affected by the attractions of neighboring stars, they will then compose a separate system, and remain united by the bond of their own mutual gravitation towards each other. This should be called a real double star; and any two stars that are thus mutually connected, form the binary sidereal system which we are now to consider."

Nowadays the term ''binary star'' is used in order to describe a stellar system that consists of two stars orbiting around a common center of mass. The most massive star is usually referred to as ''primary star'' and the other one as ''secondary star''. Recent research has shown that many stars are part of either binary stellar systems or stellar systems with more than two stars. In 1767 John Michael first suggested that double stars might be physically attached to each other. About ten years later, in 1779 William Herschel began observing double stars and in 1827 Felix Savary computed the first hole orbit of the double star Xi Ursae Majoris.

Today it is known that binary stars are classified into four types according to the way in which they are observed:

- Visual Binaries

- Spectroscopic binaries (periodic changes in spectral line)

- Photometric binaries (changes in brightness caused by an eclipse)

- Astrometric binaries (by measuring a deviation in a star's position caused by an unseen companion.)

1.1.2 The Roche lobe

Binary stars can sometimes interact by transferring mass from the one star to the other. Roche lobe represents a region of space around a star in a binary system within which orbiting material is gravitationally bound to that star. The term Roche lobe has been chosen to honor the French mathematician Eduard Roche (1820-1883). If the material overflows the Roche lobe, then it can escape from the gravitational pull of the star and it falls into the other through the inner Lagragian point creating an accretion disk.
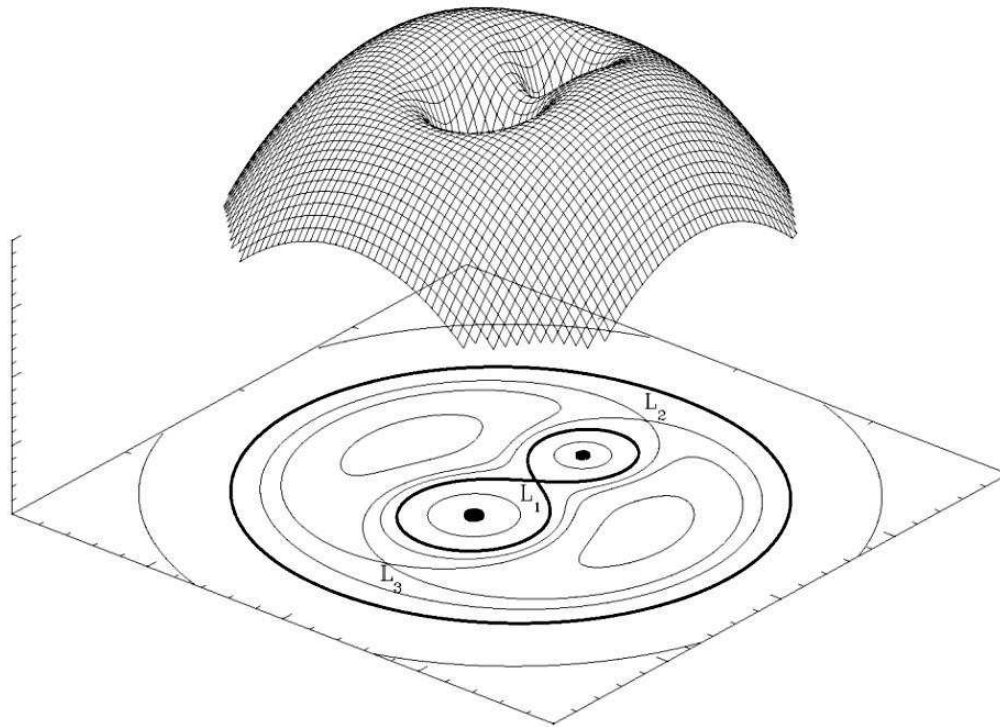
Figure 1.1: A three-dimensional representation of the Roche potential in a binary star with a mass ratio of 2. L_1, L_2 and L_3 are the Lagrangian points where forces cancel out. Mass can flow through the saddle point L_1
From the one star to each companion if the star fills its Roche lobe (http://en.wikipedia.org/wiki/Roche_lobe)

The Lagrangian points are five places in the orbital plane of the binary system where kinetic and potential energy are equal. In binary systems the most important point is the inner lagrangian point (L_1) where the two Roche lobes meet (Figure 1.1). The matter can escape from the one star and reach the inner lagrangian point in two ways. The first one is the strong stellar wind. If the star has a strong stellar wind, some of the gas can get away from it and pass through the inner lagrangian point to the other star. Then, the other star will capture some of this gas. Secondly, if the star expands so far and fills its Roche lobe, then the matter can overflow through the inner lagrangian point the other star (Seeds &Backman 2012).

1.2 General properties of X-ray binaries

1.2.1 Definition of X-ray Binaries

X-ray binary stars is a category of binary stars that are luminous in X-rays. The X-rays are produced by matter falling from one component, usually a normal star, called donor star, to the other component, called the accretor. The accretor is a compact object such as a white dwarf, a neutron star, or a black hole and it is orbiting the optical companion. By ''optical companion'' we refer to a star with nuclear burning taking place in its interior. X-ray binaries are close binary systems because of a transfer of mass from the optical component to the compact object. If the compact object (the accreting star) is a neutron star or a black hole, the matter falls onto an enormous well of gravitational potential and is accelerated to extremely high velocities. When the matter reaches the surface of the neutron star (or the black hole), it decelerates and the free fall kinetic energy is radiated away as heat which is available to power the X-ray source (Frank et al. 2002). The orbital period of HMXBs ranges from one day to one year in contrast with LMXBs that is 10 min to 10 days. Today, we know more than 300 Galactic X-ray binaries with a luminosity of 10^{34}-10^{38}erg^{-1}. They are concentrated towards the Galactic center and the Galactic plane and some of them are found in globular clusters (Seward & Charles 2010).

1.2.2 Classification of X-ray Binaries

X-ray binaries are divided into three main categories depending on the type of the compact object (neutron star, black hole or white dwarf). An alternative classification can be accomplished based on the physical properties of the optical companion: it can be a high mass X-ray binary or a low mass x-ray binary system (Figure 1.2).

Figure 1.2: Mechanisms by which matter is transferred onto a compact object in a binary system. (top) A low-mass star has evolved and is losing mass to its degenerate companion because it fills its *Roche lobe* and mass flows through the *L* 1 point. (bottom) The compact object is orbiting a massive star which has a very powerful stellar wind (Seward & Charles, 2010).
.
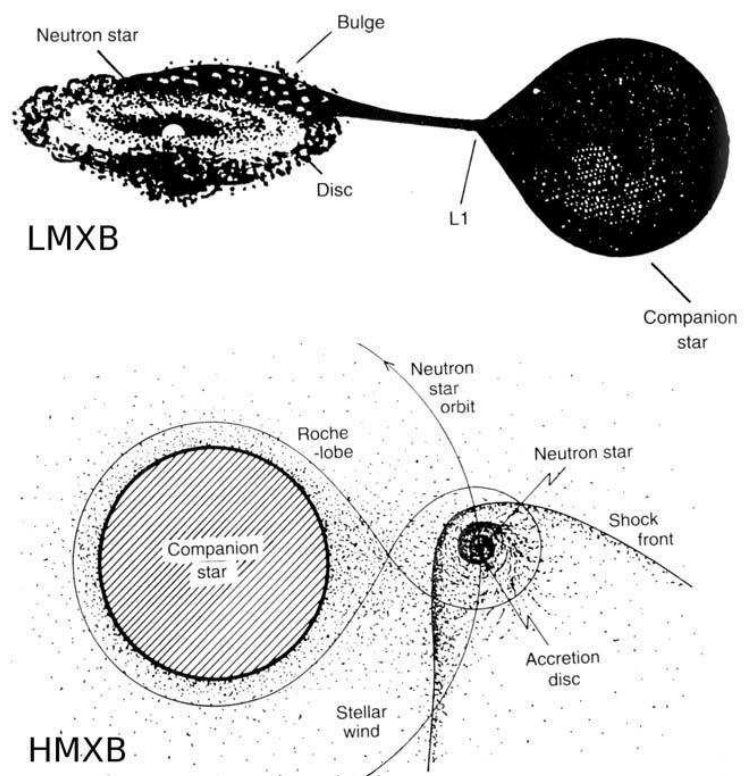
In a *low mass X-ray binary* (LMXB), the donor star is less than 3 solar masses ($M < 3M_o$). Approximately, one hundred LMXBs have been detected in the Milky May and of these, thirteen have been discovered in globular clusters. In LMXBs the compact object is either a black hole or a neutron star. The donor star usually fills the Roche Lobe and therefore it transfers mass to the compact star. The donor star can be on the main sequence, a white dwarf, or a red giant.

High mass X-ray binaries (HMXBs) are binary systems in which the donor star is a massive star of spectral type O or B. The compact object is typically a neutron star but it can also be a black hole, or a white dwarf.

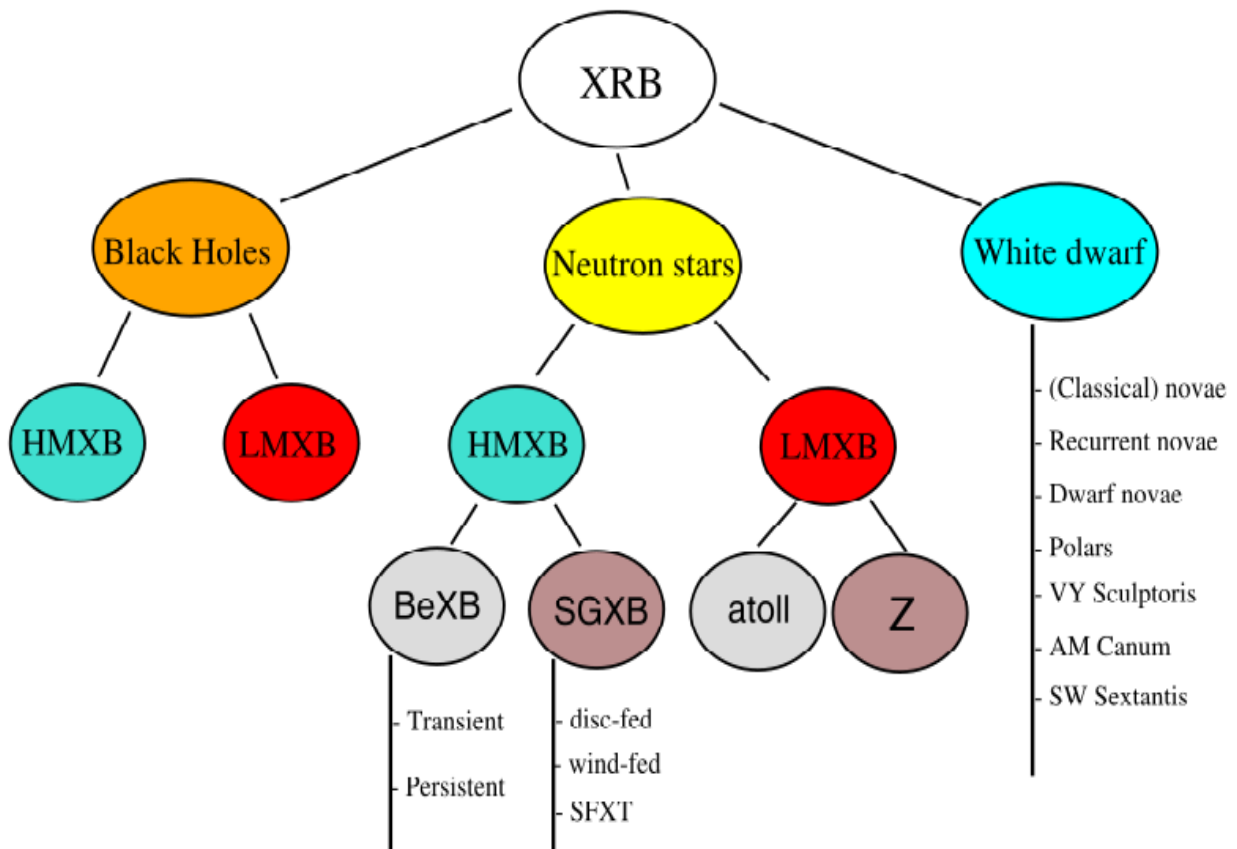The classification of X-ray binaries is given in Figure 1.3.

Figure 1.3: Classification of Be/X-ray binaries, Reig (2011)

1.3 High mass X-ray binaries (HMXBs)

1.3.1   General characteristics

When talking about HMXBs we mean a system of a compact object orbiting around an early-type star (O or B) and emit X-ray radiation. A fraction of the stellar wind of the massive normal star is captured by the compact object, and produces X-rays as it falls onto the compact object. In a high-mass X-ray binary, the massive star dominates the emission of optical light, while the compact object is the dominant source of X-rays. Sometimes they appear as the brightest objects of the X-ray sky.

1.3.2 Classification of HMXBs

HMXBs are divided into two major groups according to the luminosity class of the optical companion. They are subdivided into Be/X-ray binaries (BeXs) when the optical star is a main sequence or giant star (i.e. luminosity class III, IV or V) and supergiant X-ray binaries (SGXBs) if the donor star is an evolved star and luminosity class I, II.

Supergiant X-ray binaries (SGXBs) were the first discovered HMXBs because of their brightness and strong X-ray emission. In SGXBs the optical star emits a stellar wind, with mass-loss rate of 10^6-10^8 $M_\odot$ yr^{-1} and a terminal velocity up to 2000 km s^{-1}. SGXB are subdivided also into low luminosity or wind-fed systems and high-luminosity or disk-fed systems. Disk-fed SGXBs show short orbital periods and short spin periods. They display an anticorrelation in the P_{orb}-P_{spin} diagram (Figure 1.4). Wind-fed SGXBs show long spin periods and short orbital periods. They sit in a flat region in the P_{orb}-P_{spin} diagram, commonly referred to as the "Corbet's diagram" (Corbet 1986). Today, only three disc-fed SGXB are known and just one of them was found in the galaxy (Cen X-3) and a few dozens of wind-fed SGXBs have in total been detected.
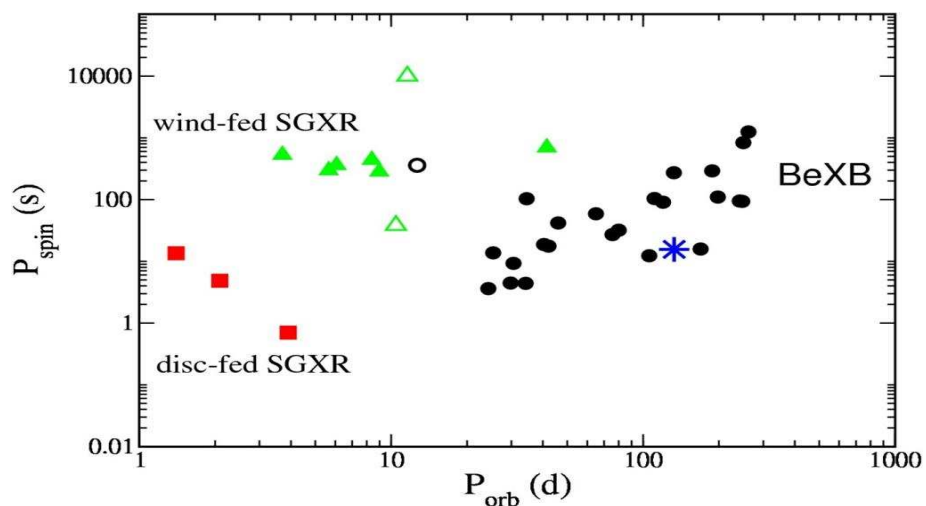

Figure 1.4: Extension of Corbet's diagram (Be/X-ray binaries, Reig (2011))

Be/X-ray Binaries (BeXB) is a category of X-ray binaries where the optical companion is a Be star. The symbol Be refers to a star of spectral type B and the letter "e" shows that sometimes spectral lines appear in emission. The emission lines come from a decretion disc around the Be star. It is important to remark that BeXBs show a linear correlation in the P_{orb}-P_{spin} diagram.

1.3.3 Persistent and transient X-ray sources

Most BeXB are transient systems in the sky moderately eccentric orbits ($e \geq 0.3$). However, persistent sources also exist. The differences between persistent and transient BeXBs are the following (Reig & Roche 1999).

Persistent sources exhibit:

Figure 1.5: Schematic of a Be/X-ray Binary

- Low X-ray luminosity, $L_{2-20keV}=10^{34-35}$ erg s^{-1}.
- Relatively quiet systems showing flat curves with sporadic and unpredicted increases in intensity by less than an order of magnitude.
- Slowly rotating pulsars, $P_{spin} \geq 200$ seconds.
- Absence of, or very weak, iron line at 6.4 keV, indicative of only small amounts of material in the vicinity of the neutron star.

These X-ray properties corresponds with systems with wide ($P_{orb} \geq 200$ days) and low eccentricity orbits ($e \leq 0.2$).

On the other, the X-ray behavior of transient BeXB is characterized by two type of outbursting activity:

- Type I outbursts refers to regular and periodic (or quasi-periodic) outbursts. They are normally peaking close to periastron passage of the neutron star. They are short-lived and the X-ray flux increases by about one order of magnitude with respect to the pre-outburst state, reaching peak luminosities $L_x \leq 10^{37}$ erg s^{-1}.
- Type II outbursts, on the other, shows major increases of the X-ray flux. They reach the Eddington luminosity for a neutron star and become the brightest objects in the X-ray sky. For different orbital periods they do not show any preferred phase. An accretion disk can also be created by in type II outbursts.

Figure 1.6 below shows these two types of X-ray variability

Figure 1.6: Type I and type II outbursts in EXO 2030+375 and 4U 0115+63.

1.3.4 The Bondi-Hoyle accretion

Bondi-Hoyle accretion is the accretion of material by a body travelling through a uniform density medium such as interstellar space (Bondi & Hoyle, 1944). It can be applied to a compact object moving in a stellar wind as in the case of the massive X-ray binaries. The geometry of this problem is shown in figure 1.7.
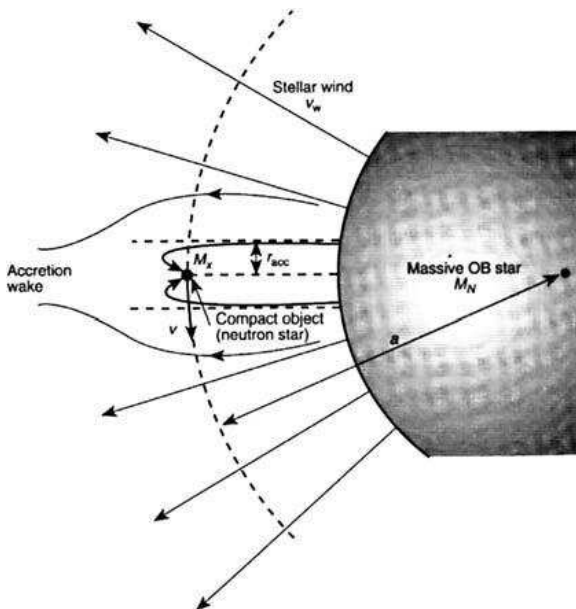
Figure 1.7: Geometry of accretion onto a compact object orbiting its massive companion. The wind of material leaving uniformly in all directions from this star's surface will accrete onto the neutron star only if it is within a critical distance (r_{acc}) of the compact object, thereby forming an *accretion cylinder*. Material that is perturbed in its flow but does not actually accrete forms an *accretion wake* beyond the compact object (Seward & Charles, 2010).

The wind of the massive star flows out uniformly in all directions. Material in a cylinder of radius r_{acc} will be accreted by the compact object while material outside of the cylinder will escape. Material will only be accreted if it has a kinetic energy less than the potential energy in the vicinity of the compact object which has a mass M_x. Consequently, r_{acc} is given by solving the following equation:

$$\frac{1}{2}mu_{rel}^{2} = \frac{GM_x m}{r_{acc}}$$

where u_{rel} is the relative velocity of the compact object and the stellar wind.
This is computed from:

$$u_{rel}^2 = u^2 + u_w^2$$

where $u^2 = GM_n / a$ for an early type star with a mass M_n and radius of orbit α.

The amount of material accreted by the compact object is given by the amount inside the accretion cylinder, which is

$$M = \pi r_{acc}^2 u_{rel} \rho$$

Where ρ is the density and can be calculated from the assumption that the wind is uniform,

$$\rho = \frac{M_w}{4\pi\alpha^2 u_w}$$

Solving these equations the result is the fraction of the wind that is accreted.

$$\frac{\dot{M}}{\dot{M}_w} = \left(\frac{M_x}{M_n}\right)^2 \frac{(u/u_w)^4}{\left[1+(u/u_w)^2\right]^{3/2}}$$

1.3.5 The power of accretion

If the compact object of mass M is accreting material at a rate dM/dt, then the luminosity resulting from this accretion is:

$$L = \frac{GM(dM/dt)}{R}$$

where most of this energy is liberated near the object's surface.

Comparing the efficiency of this energy for three types of compact object with that for nuclear energy and expressing the luminosity obtained from the given mass accretion rate as a fraction of the total energy that the matter possesses, it is possible to find that

$\eta=0.1$ for neutron stars
$\eta=0.06\text{-}0.42$ for black holes
$\eta=0.001$ for white dwarfs
$\eta=0.01\text{-}0.001$ for nuclear reactions

where η=GM/Rc^2 and therefore the luminosity equation becomes $L = \eta \dfrac{dM}{dt} c^2$ (Seward & Charles, 2010).

1.3.6 The Eddington Limit

The Eddington limit refers to the maximum luminosity that a star can have and still remain in hydrostatic equilibrium. The Eddington luminosity limit is given by

$$L_{Ed} = \frac{4\pi GMm_p c}{\sigma_o}$$

where σ_o is the Thomson cross section. If the luminosity L of a star approaches the Eddington luminosity limit L_{edd} then it is possible for radiation pressure to overcome the gravitational force of a compact object and thereby stop the accretion of the matter. Putting the constants in the equation above gives:

$$L_E = 1.3 \times 10^{38} \frac{M}{M_\odot} \, erg \cdot sec^{-1}$$

This means for example that a neutron star of mass $1.5\,M_\odot$ cannot produce a steady luminosity greater than about $2 \times 10^{38} erg \cdot sec^{-1}$.

1.4 Be/ X-ray binaries (BeXBs)

1.4.1 Physical properties of BeXBs

The most numerous class of Massive X-ray Binaries in the galaxy are composed of Be stars and neutron stars. These systems contain two quasi-Keplerian disks. A decretion disc exists around the Be star and an accretion disc around the neutron star (Ziolkowski 2002). Optical spectroscopic observations of Be stars have shown that spectral lines appear occasionally in emission. Hα in emission is the best studied line but also He, Fe lines in emission have been detected (Hanuschik 1996). In addition, Be/X-ray Binaries show IR radiation to be larger than expected from typical B star of the same spectral type (infrared excess). The emission lines and infrared excess in BeXB are caused by a circumstellar gaseous component which can be an equatorial disc. The mechanism responsible for the production of the circumstellar gas is still not fully understood (Porter and Rivinius 2003).
The X-ray radiation is powered by the infalling matter of the decretion disc of the Be star onto the neutron star when it passes through periastron. The conversion of the kinetic energy of the in-falling matter into radiation powers the X-rays. Also, a Be star can

overflow the Roche lobe and then the matter falls through the Lagrangian point creating an accretion disc. This is expected occur in Type II outbursts.
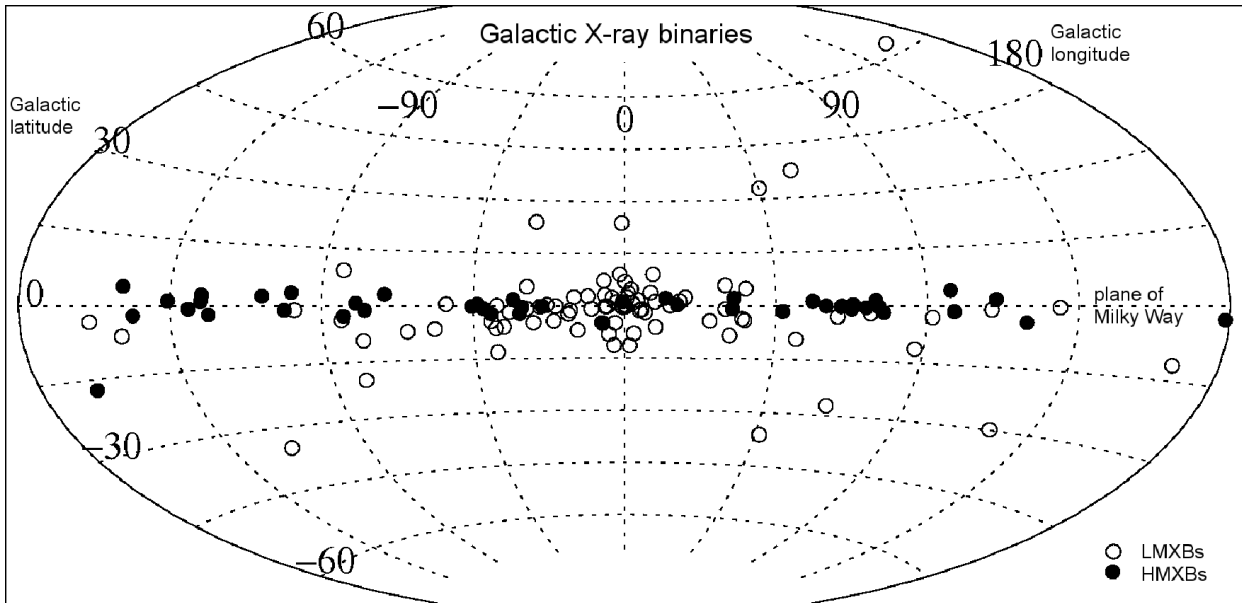
Figure 1.8: Distribution of X-ray binaries on the sky, plotted in galactic coordinates. HMXBs (filled circles) are located in the spiral arms, in the plane of the Galaxy. LMXBs (open circles) are much older and are in the Galactic Bulge (Seward & Charles, 2010).

As mentioned previously, BeXB are distributed on the Galactic plane, indicating that the majority belong indeed to our Galaxy and also that these stars are early type stars. Table 1.1 shows the systems with indentified optical counterparts and whose X-ray and optical/IR variability has been shown to be typical of BeXB (Reig 2011).
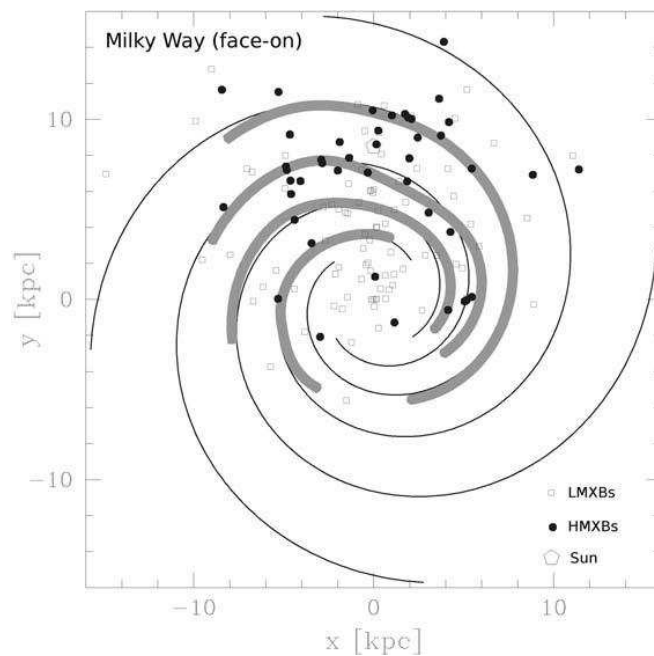
Figure 1.9: Face-on view of the distribution of X-ray Binaries in the Galaxy (Seward & Charles, 2010).

Table 1.1: Statistics in HMXBs in the Milky Way (Reig 2011).

Statistics on HMXBs in the Milky Way	
Number of neutron star X-ray Binaries	327
Number of suspected HMXB	131
Number of suspected BeXB	63
Number of confirmed BeXB	28

1.4.2 Optical properties of BeXBs and the Hα line profile

Optical observations of BeXBs can reveal the physical state of the donor component but also give information about the physical conditions under which the compact object is accreting. The circumstellar envelopes of ionized gas around the equator of the Be star produces emission spectral lines. The Hα line is the main parameter to give information on the circumstellar disk. By measuring Hα emission line profile it is possible to obtain important constraints on the geometry and dynamics of the envelopes (Hanuschik 1986).
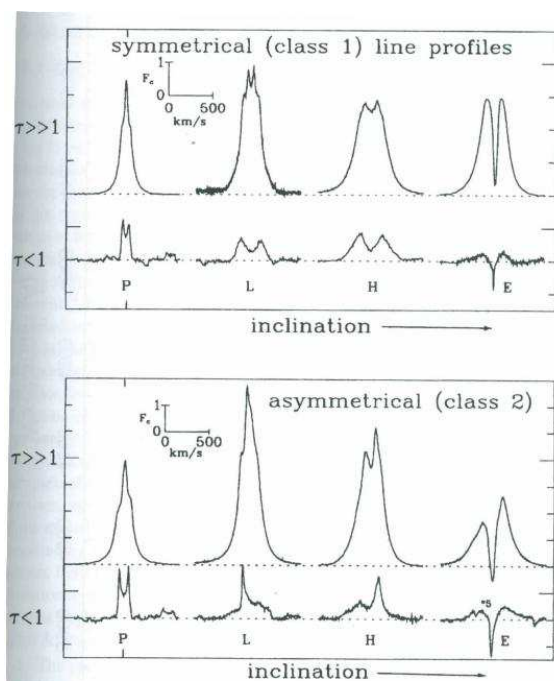
Figure 1.10: Typical emission-line shapes for symmetrical and asymmetrical profiles on the Hanuschic et al. (1996) classification system for Be stars.

Hα emission lines can be divided into two classes based on the morphology of their profile. Class 1 include the symmetric line profiles while class 2 include asymmetric profiles with variability on time scales of years (Figure 1.10& 1.11). Be stars can change from the one class to the other. Isolated Be stars can exibit this change in time scales of years to decades but the Be stars in BeXB systems can vary in duration from some months to some years.

Most Be stars show asymmetric Hα line profiles. V/R variability refers to the variation of the relative strength of the blue to the red peak and it is a crucial characteristic of the Hα line profiles of BeXBs. The peaks adopt the names of the relative position of their central wavelengths. V/R ratio is defined as the ratio of blue peak to red peak intensities above the continuum and it represents a measure of the asymmetry of line. In practice it is common to use the logarithm of this ratio, log(V/R).
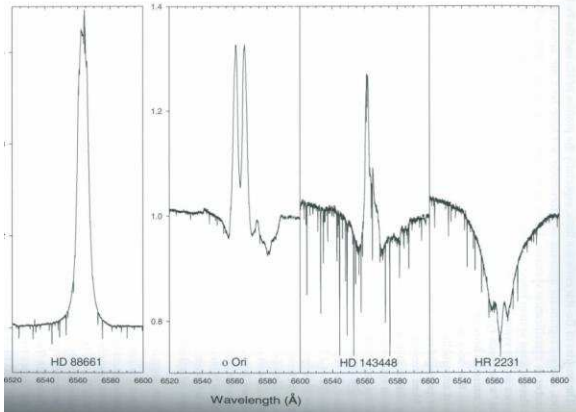
Figure 1.11: Some examples of Hα line profiles in Be stars (R. O. Gray, C. J. Corbally, (2009).

V/R variability is explained by a density perturbation which revolves in the disk. Double peak asymmetric profiles are expected when the high density part is behind or in front of the star, while asymmetric profiles are seen when the high density perturbation is on one side of the disc. The high-density part is a term used to describe a zone in the disk with higher density and it is common to use it in order to explain V/R variability phenomenon. Enhanced red emission (V<R) is detected when the high-density part of the disc perturbation is located on the side of the disc where the rotation motion is directed away from us and when it is moving toward to us a blue-dominated profile (V>R) is observed (Reig 2011).

V/R variability is also seen in other lines, like He I 6678Å. In the figure below the V/R variability is observed in the Ha line of LSI +61 235 (Reig et al. 2000
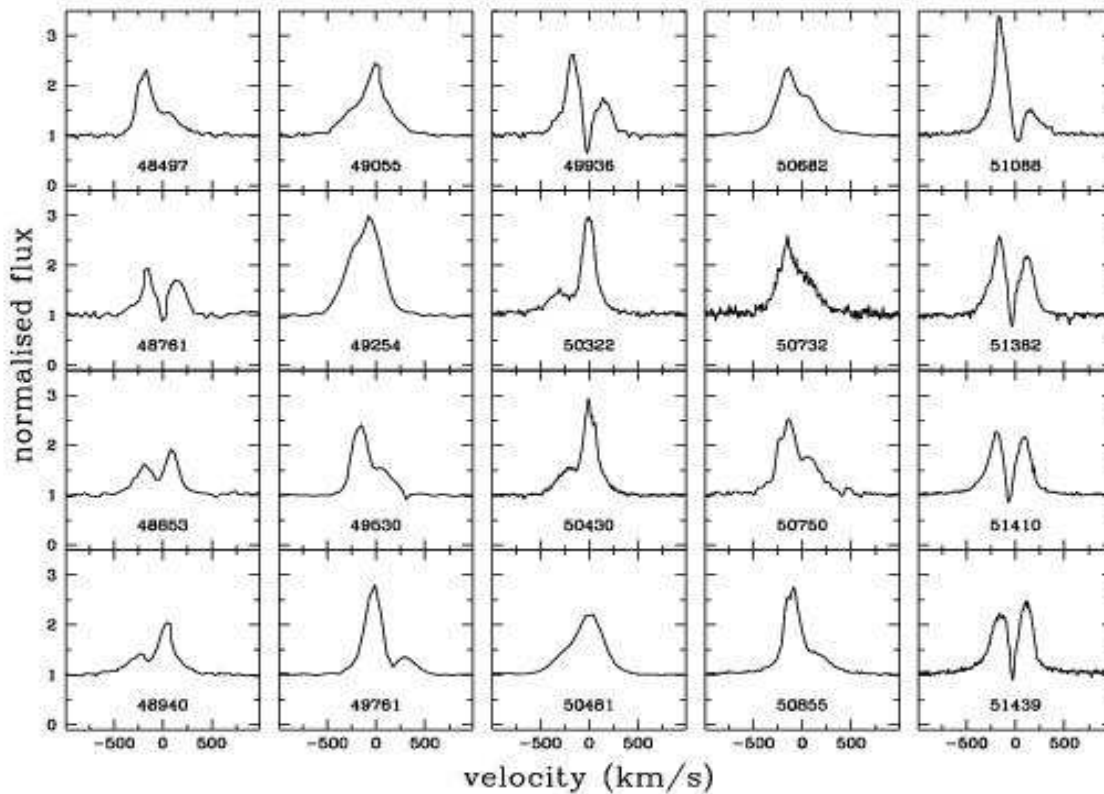
Figure 1.12: V/R variability observed in the Ha line of LS I+61 235. Reig et al. (2000)

1.5   Decretion disk

1.5.1   The disc formation

Be stars are rotating in very large rotational velocities close to the critical velocity (the velocity at which centrifugal forces balance gravity). The rotational velocity constitutes an important parameter in the formation of the circumstellar disk. The projected rotational velocities are determined by measuring the width of certain spectral lines. The width of spectral lines and the rotational velocity are linearly related (Reig 2011).

The origin of the gas in these disks seems to be material ejected from the stellar photosphere. However, the exact mechanism that causes this mass ejection has not been defined yet. Many models have been suggested in order to explain the disc formation.

The main idea in the *wind-compressed model* is that in a rotating wind, the material tends to orbit the star during the time it is accelerating outward. If the outward acceleration is small compared to the rotation, then the radiation-driven wind flows toward the equator.

The *magnetically torqued model* extends the ideas of the wind compressed disc model by adding magnetic steering and torquing up of the angular momentum of the wind. The up-flowing wind from near the star is magnetically channeled back to the equator. It requires a dipole-like magnetic field to channel the flow of the wind material into a disc region along the equatorial plane.

1.5.2   The disc loss phenomenon

Some of Be stars display a disk loss episode. This means that their deccretion disk disappears at some point of their life. This phenomenon is important to indentify the real luminosity of the Be star and the luminosity of the disk. Spectroscopic and photometric observations of Be stars indicate additional reddening caused by hydrogen free-bound and free-free processes in the circumstellar envelope in comparison to the non-emission B stars. When the disk from the Be star disappears then it is possible to measure the real luminosity of the star.
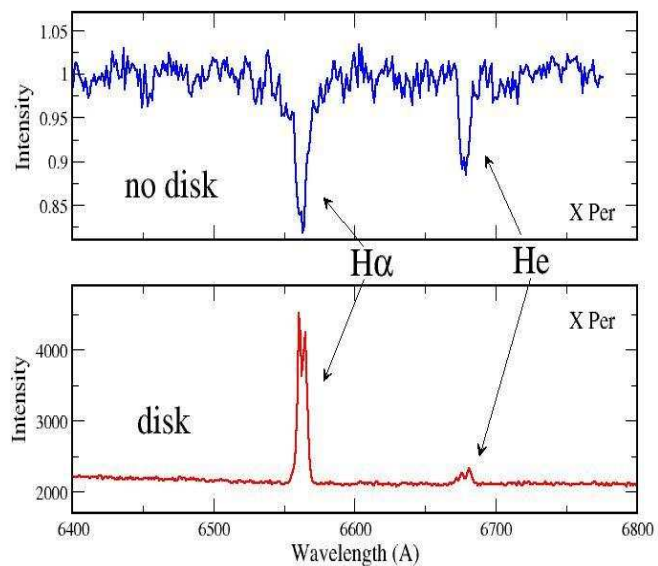
Figure 1.13: The Hα and He line profiles. Up: Absorption Down: Emission (Reig 2011).

The luminosity taken from the star with the disk minus the luminosity without the disk can give the luminosity from the disk. Hα line is the prime indicator of the existence or not of the disk. When the star loses the disk, the Ha line shows an absorption profile and when it appears again the Ha is in emission. These two phases are presented in figure 1.13.

1.6 Aims of the project

The main goal of this work is to study the long-term optical properties of the optical counterpart to the X-ray source IGR J21343+4738. For the aims of the project observational data were taken from Skinakas Observatory in Crete. Also data from the Fred Lawrence Whipple Observatory (FLW) at Mt. Hopkins (Arizona) and from William Hershel Telescope (WHT) of El Roque de los Muchachos observatory in La Palma (Spain) were used. Spectroscopic observations of IGR J21343+4738 were analyzed in order to determine the physical parameters of the Be star. More specifically, the purpose of the project is:

a. to examine the disk variability of the optical counterpart to the X-ray source IGR J21343+4738 and the report of a disk loss episode.
b. to find the spectral type of the Be star.
c. to determine the rotational velocity of the Be star.
d. to estimate the disk radius.

Finally, a discussion of the results is presented.

Chapter 2

Observations

Optical spectroscopic observations of the optical counterpart to the INTEGRAL source IGR J21343+4738 were carried out from Skinakas Observatory (SKO) in Crete. Skinakas Observatory was founded by the University of Crete, the Foundation for Research and Technology - Hellas (FORTH) and the Max Planck Institut fuer Extraterrestriche Physik, Germany. Skinakas observatory owns three telescopes. A 1.3m modified Ritchey–Chrétien telescope, a 0.6m remotely controlled telescope and a 0.3m Schmidt-Cassegrain telescope. At the present project the observations have been made using the 1.3 meters Telescope. Also, IGR J21343+4738 was observed from the Fred Lawrence Whipple Observatory (FLW) at Mt. Hopkins (Arizona) and from the 4.2 meters William Hershel Telescope (WHT) of El Roque de los Muchachos observatory in La Palma (Spain).

The 1.3 meters Skinakas telescope was equipped with a slit spectrograph and a 2000x800 ISA SITe CCD camera. For the ongoing project we used the 1302 mm^{-1} or 2400 mm^{-1} grating (see fig1). Also IGR J21343+4738 was observed in queue mode with the 1.5 meters telescope (FLW) and the FAST-II spectrograph plus FAST3 CCD, a backside-illuminated 2688 x 512 UA STA520A chip with 15μm pixels. Moreover, the WHT observations were taken in service mode with the ISIS spectrograph and the R1200B grating.

2.1   The 1.3 meter Skinakas telescope

The 1.3 meter telescope is the principal observing facility of Skinakas Observatory. The technical details are presented below.

- Aperture of main mirror: 129cm

- Aperture of secondary mirror: 45cm

- Central hole of main mirror: 35cm

- Distance main to secondary: 245.34cm

- Focal length: 985.7cm

- F-ratio: 7.64
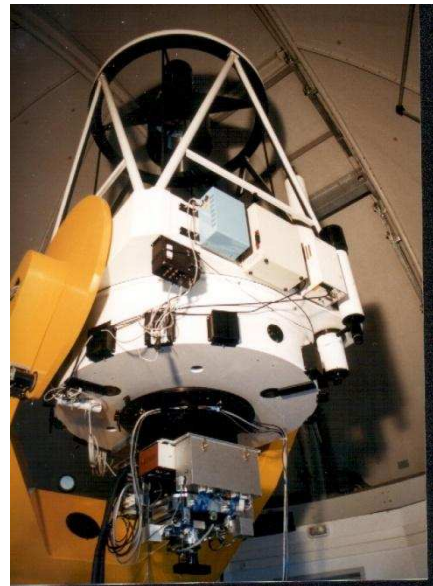
Figure 2.1: Skinakas 1.3 meter telescope.

2.2 Other equipment

2.2.1 Focal reducer and slit spectrograph

A Focal Reducer is mounted to the 1.3m telescope. The Focal Reducer can be used in two different configurations:

1. In the imaging mode the focal length of the telescope is reduced by a factor of 1.87, enlarging by the same factor the imaged area of the sky on the CCD. A Filter Wheel with 6 filter positions is integrated to the Focal Reducer.
2. In the spectroscopy mode a reflection grating is introduced in the collimator path. Using different gratings, resolutions ranging from 0.57Å/pixel to 4Å/pixel are achievable with a 15µm pixel CCD camera. A Slit Wheel offering 6 positions with slit widths: 80µm, 160µm, 320µm and 640µm is part of this configuration.
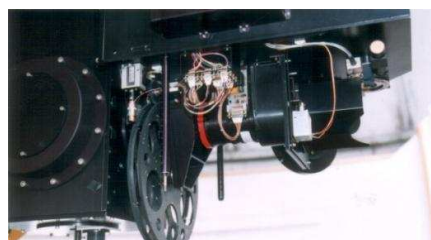
Figure 2.2: Up: Front view,
Down: side view

The gratings for the focal reduced used for the observations are presented in the table below.

Table 2.1: Grating for the focal reducer

Lines/mm	Zero order blaze wavelength (nm)	Dispersion (Å/nm)	Mounted
1200	700	76.39	Yes
1302	430	70.44	Yes
1302	550	70.27	Yes

2.2.2 Charge couple device, CCD

During the measurements, a Jobin Yvon, (currently Horiba) CCD camera was used. The camera is attached to the slit spectrograph. Additional characteristics of the CCD camera are presented in the next table.

Table 2.2: Characteristics of CCD camera

Model name	Dimension (pixel)	Pixel size (µm)	Image area (mm)
ISA 608	2000x800	15	30x12

2.3   Observation field

The observation field of IGR J21342+4738 is presented below. The image was processed with the image editor for Linux, *DS9*. The source is indicated by the red vectors. The North is up and the East is left and the coordinates of the source are shown on the image.
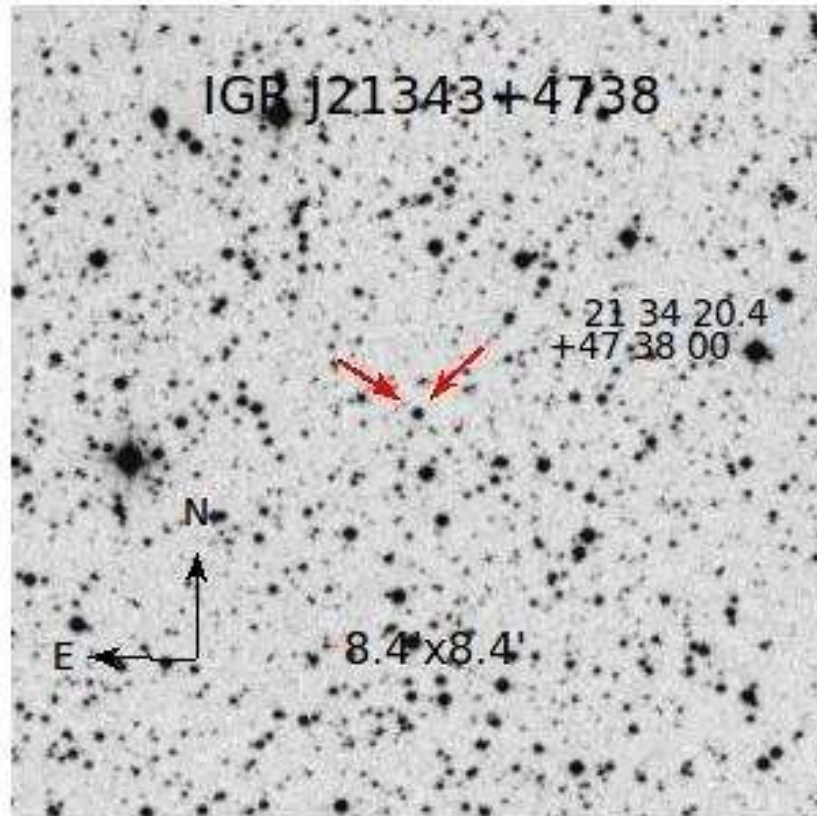
Figure 2.3: Observation field

2.4 Table of Observations

More details on the observation data are presented in the tables below.

Table 2.3: Log of the spectroscopic observations around the Hα line.

Civil date	JD(2400000+)	Telescope	Grating (mm^{-1})	Wavelength coverage(Å)	Dispersion (Å/pixels)
30/7/2009	55043.41	SKO	1302	5300-7370	1.04
29/9/2009	55104.37	SKO	2400	6070-6985	0.50
28/8/2010	55437.41	SKO	1302	5305-7380	1.04
30/9/2010	55470.39	SKO	1302	5225-7295	1.04
20/8/2011	55794.45	SKO	1302	5210-7290	1.04
6/9/2011	55811.29	SKO	2400	6080-6995	0.45
24/8/2012	56164.41	SKO	1302	5090-7160	1.05
6/9/2012	56177.46	SKO	1302	5530-7590	1.04
13/9/2012	56184.40	SKO	1302	5420-7500	1.04
15/10/2012	56216.31	FLW	1200	6200-7200	0.83
19/10/2012	56220.31	SKO	1302	4750-6820	1.04
26/12/2012	56288.21	WHT	1200	6370-7280	0.25
4/1/2013	56297.07	FLW	1200	6200-7200	0.37
11/1/2013	56304.08	FLW	1200	6200-7200	0.37
15/6/2013	56459.53	SKO	1302	4960-7030	1.04
5/7/2013	56477.35	FLW	1200	6200-7200	0.83
31/7/2013	56505.45	SKO	1302	5400-7480	1.04
23/8/2013	56527.50	WHT	1200	6350-7240	0.75

Table 2.4: Log of the spectroscopic observations in the blue region.

Civil date	Julian date	Telescope	Wavelength coverage (Å)
26/12/2012	2456288	WHT	3870-4670
23/8/2013	2456528	WHT	3840-4670

2.5   Data processing

The spectra used for the present project were already reduced. Their reduction and performed can be made using the proper packages of IRAF project. Firstly, the raw images were BIAS subtracted and FLAT field corrected. A BIAS frame is an image obtained with no actual exposure time. The image so obtained only contains noise due to the camera electronics and not noise from charge accumulation within the sensor itself.

FLAT field correction is a technique used to improve quality in digital imaging. The goal is to remove artifacts from 2-D images that are caused by variations in the pixel-to-pixel sensitivity of the detector.

Also spectra of comparison lamps are taken before each exposure. This technique helps to perform the wavelength calibration during the night. The last correction is the sky subtraction. The sky subtraction is carried out by measuring the sky spectrum.

Finally, all the spectra were normalized with the local continuum in order to obtain a homogenous processing of the spectra.

Chapter 3

Data analysis and Results

In this part of the project the results generated from the data analysis are presented. Optical spectroscopic observations since 2009 were used in order to observe the long-term variability of the optical counterpart to the X-ray source IGR J21343+4738. The monitoring of the Hα line profile is the prime indicator of the state of the circumstellar disk. The blue spectra were also used in order to determine the spectral type of the optical companion.

3.1   Monitoring the Hα line profile

The aim of this part of the data analysis is to study the variability of the disk on timescales of months to years. By observing the Hα line profile we can understand the state of the circumstellar disk and also we can follow the variability of this line, both in strength and shape. More specific, by measuring the EW(Hα) (see Appendix A) of the Hα line we can obtain information about the size of the circumstellar disk. The results obtained by analyzing the Hα line spectra of IGR J21343+4738 from 2009 to 2013 are presented in table 3.1. All the spectra were analyzed using the *splot* task of the Image Reduction and Analysis Facility, *IRAF*.

Table 3.1: Results of the Hα line profile analysis.

Date	Julian Date 2.400.000+	λ(V) Å	λ(R) Å	Δpeak (km s^{-1})	log(V/R)	EW (Hα)
30/7/2009	55043.41	6553.1±0.2	6567.1±0.4	635±21	0.1±0.2	1.4±0.13
29/9/2009	55104.37	6555.1±1.2	6567.2±0.5	553±58	-0.4±0.2	0.8±0.6
28/8/2010	55437.41	6554.8±0.3	6567.3±0.3	571±20	0.07±0.05	0.5±0.2
30/9/2010	55470.39	6554.7±0.3	6566.0±0.1	515±16	0.11±0.06	0.22±0.13
20/8/2011	55794.45	6556.4±0.2	6565.7±0.1	425±10	-0.05±0.01	-0.74±0.27
6/9/2011	55811.29	6554.6±0.4	6565.1±0.2	478±18	-0.16±0.06	-1.8±0.7
24/8/2012	56164.41	6555.62±0.04	6563.5±0.1	360±5	0.38±0.01	-8.5±0.9
6/9/2012	56177.46	6557.93±0.04	6565.4±0.1	341±4	0.31±0.01	-10.6±1.47
13/9/2012	56184.40	6557.4±0.1	6566.9±0.2	436±78	0.39±0.02	-7.8±1.17
15/10/2012	56216.31	6557.98±0.04	6565.5±0.1	340±45	0.001±0.010	-5.2±0.4
19/10/2012	56220.31	6555.7±0.1	6563.5±0.1	359±5	0.15±0.01	-5.04±0.71
26/12/2012	56288.21	6554.5±0.1	6564.04±0.02	438±5	-0.84±0.02	-2.1±0.7
4/1/2013	56297.07	6554.0±0.3	6564.92±0.04	500±12	-0.98±0.07	-1.2±0.3
11/1/2013	56304.08	6556.0±0.60	6565.0±0.1	413±27	-0.81±0.07	-0.49±0.2
15/6/2013	56459.53	-	-	-	-	2.3±0.3
5/7/2013	56477.35	-	-	-	-	1.4±0.44
31/7/2013	56505.45	-	-	-	-	1.9±0.4
23/8/2013	56527.50	-	-	-	-	1.7±0.1

Table 3.1 shows the results by fitting Gaussian functions to the Hα line profiles. It was frequent required to fit 3 Gaussian components (two in emission and one in absorption). Although in the last four measurements only one Gaussian fitting profile was needed. The errors of λ(V), λ(R), V and R were calculated by the errors mode in *splot*. Columns 3 and 4 show the wavelength of the blue and the red peak respectively. Column 5 gives the peak separation, Δpeak, between the blue and the red peak. The peak separation is defined as the deference between the central wavelengths of the red minus the blue peak in velocity units $\left(\frac{\Delta\lambda}{\lambda}\times c\right)$, where c is the speed of light. The value Δλ were calculated from the Gaussian fits. Δλ is the wavelength of the blue peak (V) minus the red peak (R) and λ is the wavelength of the Hα line (6563Å). The errors of peak separation were calculated by the error propagation method. The resulting equation is:

$$\mathrm{Err}\Delta_{\mathrm{peak}} = \frac{c}{\lambda}\sqrt{\Delta\lambda_{\mathrm{v}}^{2} + \Delta\lambda_{\mathrm{R}}^{2}}$$

Column 6 shows the ratio between the core intensity of the blue and red peaks. The log(V/R) ratio is computed as the logarithm of the ratio of the relative fluxes at the blue and red peak maxima. The errors were calculated by the error propagation method.

$$\Delta\left(\log\frac{V}{R}\right) = \frac{R}{V}\cdot\frac{1}{\ln 10}\cdot\Delta\left(\frac{V}{R}\right)$$

where

$$\Delta\left(\frac{V}{R}\right) = \sqrt{\left(\frac{\Delta V}{R}\right)^{2} + \left(\frac{V}{R^{2}}\Delta R\right)^{2}}$$

Column 7 gives the Equivalent width of the Hα line, EW(Hα), (see Appendix A). The values correspond to the average of ten measurements for a different definition of the continuum for each one and the error is the standard deviation of these values. The average value is giving by:

$$\overline{EW} = \frac{\sum\limits_{i}^{N} EW_{i}}{N}$$

and the standard deviation by:

$$S_{\overline{EW}} = \sqrt{\frac{\sum\limits_{i}^{N}(\overline{EW} - EW_{i})^{2}}{N-1}}$$

Negative values of Equivalent width means that the Hα line is fill in emission while positive values indicate absorption. Figure 3.1 shows the evolution of the Ha line profiles[1].

---

[1] All diagrams were done using the Grace graph plotting tool.
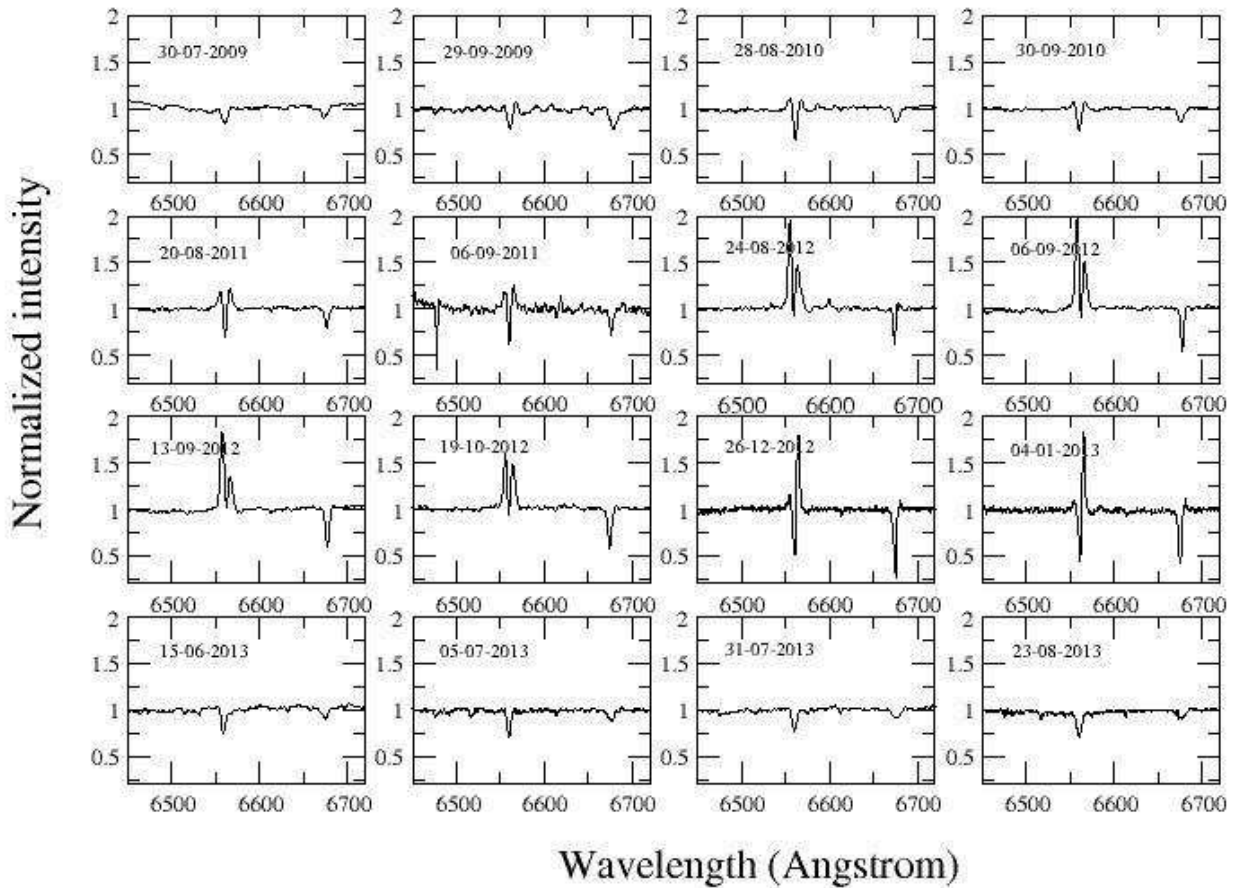
Figure 3.1: Evolution of Ha line profiles.

Figure 3.1 displays the evolution of the Hα line profile. V/R variability changes in timescales of months to years indicating significant changes in the structure of the equatorial disk. From 30-07-2009 until 06-09-2011 an absorption line profile is noted and since 24-08-2012 until 04-01-2013 an emission line profile appears. The last observations, 15-06-2013 to 23-08-2013 shows an absorption line profile.

Log(V/R) variability versus Time diagram

Figure 3.2 presents the logarithm of V/R variability as a function of time. The measurements of V/R variability were done by fitting 3 Gaussian curves in the Hα line profile (where V/R variability exists).
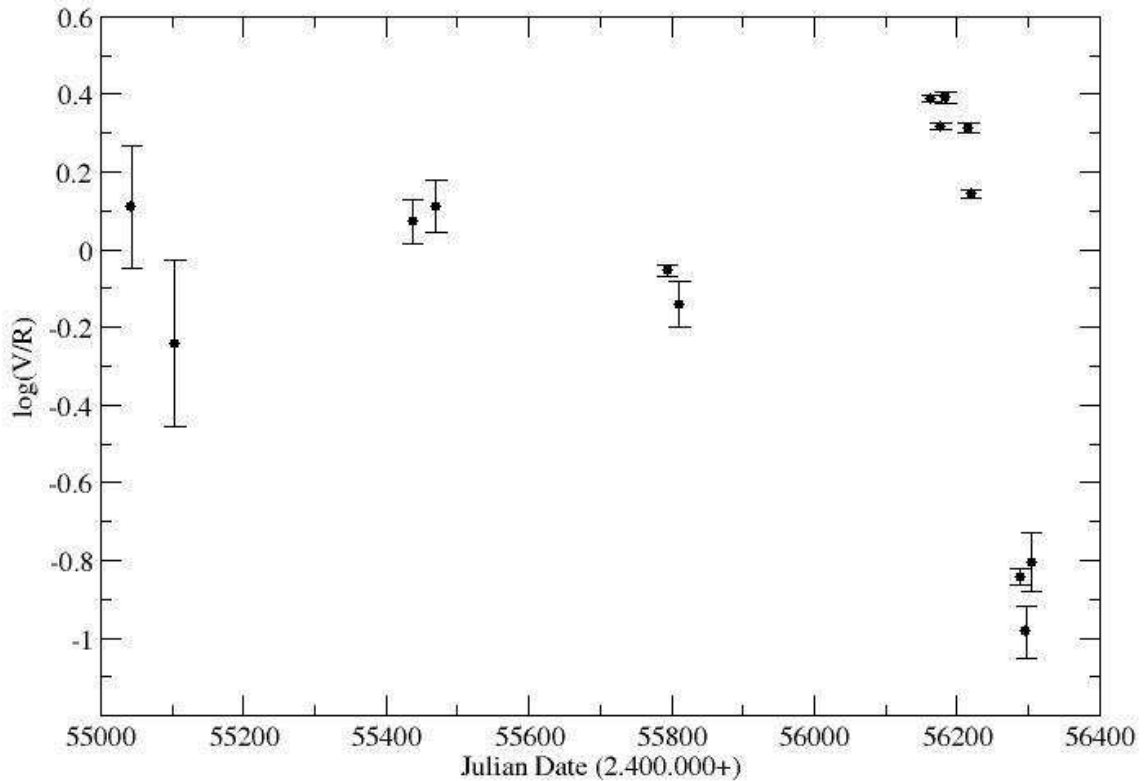
Figure 3.2: Evolution of V/R variability versus time.

V/R variability is the cyclic variation of the relative intensity of the blue (V) and the red (R) peaks in the profile of the line. This diagram shows that V/R variability changes in timescales of months confirming the previous results (Figure 3.1). The shape of the Hα line profile is changing with time indicating changes in the structure of the equatorial disk. In the first observation (30-07-2009), log(V/R) variability has a positive value and this means that the blue peak is greater than the red peak. On the contrary, the second measurement appears negative value of log(V/R) hence the red peak dominates. The following measurements are varying between positive and negative values. These values are reaching at a maximum point and then fall again below zero, at the minimum point of the diagram.

Equivalent width versus Time diagram

Figure 3.3 below presents the evolution of EW(Hα) versus time i.e. the variations of the strength of the line.
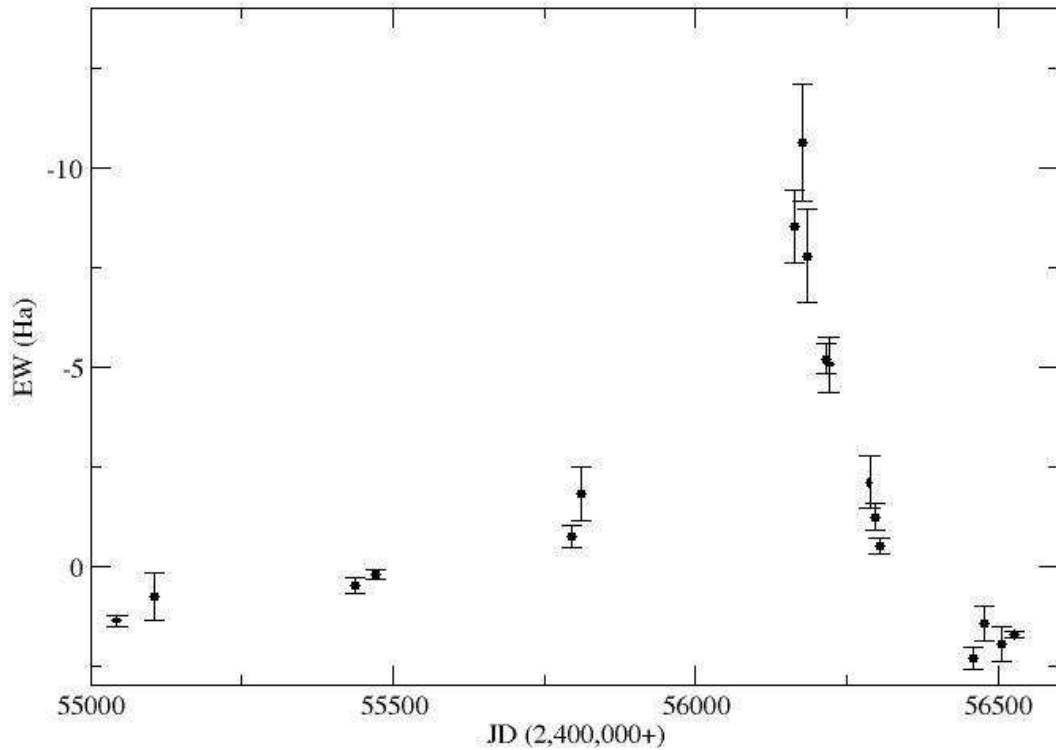
Figure 3.3: Evolution of Equivalent width versus time.

The Hα line profile appears significant changes in the strength of the line. The equivalent width increases continuously reaching a maximum point (06-09-2012) and then it starts to decrease. The first four measurements of equivalent width and the last three are positive indicating an absorption profile while negative values show an emission Hα line profile.

Peak Separation versus EW(Hα) diagram

Figure 3.4 below shows the peak separation diagram versus the equivalent width of the Hα line.
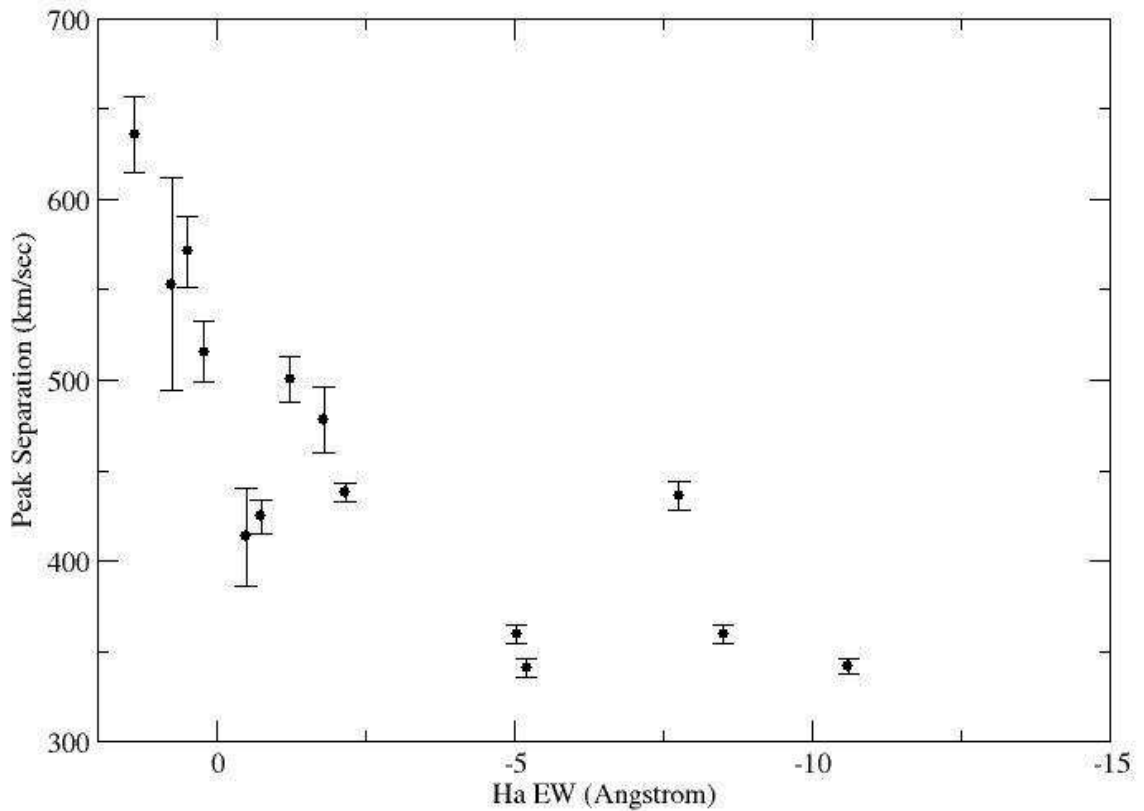
Figure 3.4: Peak separation diagram versus equivalent width.

The peak separation shows the strength of V/R variability in units of velocity. As shown from the diagram above peak separation decreases with EW(Hα). This means that the distance between the blue and the red peak increases while the line becomes fainter.

3.2   Spectral classification

Spectral classification can be done using the blue spectra, (3900-4600)Å, of IGR J21343+4738 where HeI in absorption dominates. The methodology of spectral classification is based on the identification of the spectral lines of the spectrum with that of a standard range. The standard range used for the current project is a Digital Atlas made by Walborn and Fitzpatrick, 1990.

For this purpose the spectra on Table 2.4 were used. Then the identification of the spectral lines was performed by matching the lines from the spectra of IGR J21343 +4738 with the template spectra of the atlas. The identified lines are listed in Table 3.2 below.

Table 3.2: Identification of spectral lines

Spectral line	Wavelength(Å)
He I	4009
He I	4026
CIII+OII	4072
SI IV	4116
He I	4144
He I	4387
OII	4415
He I	4471
Mg II	4481
He II	4549
Si III	4568
CIII+OII	4649

Sometimes the data have an offset of a few Angstroms in the wavelength axis. A significant offset may lead to incorrectly identified spectral lines. From the standard spectral lines (Hε, Hδ, Hγ) it is possible to find this error by measuring the wavelength of them. The difference of the measured value from the standard one gives the offset in wavelength. In the present spectra the errors were very small (~1Å) consequently no correction was needed.

Figure 3.5 shows the blue spectrum of IGR J2343+4738 and the identified lines used for spectral classification. The spectrum was smoothed in order to see the lines clearly. Figure 3.6 presents the template spectra used for spectral classification.
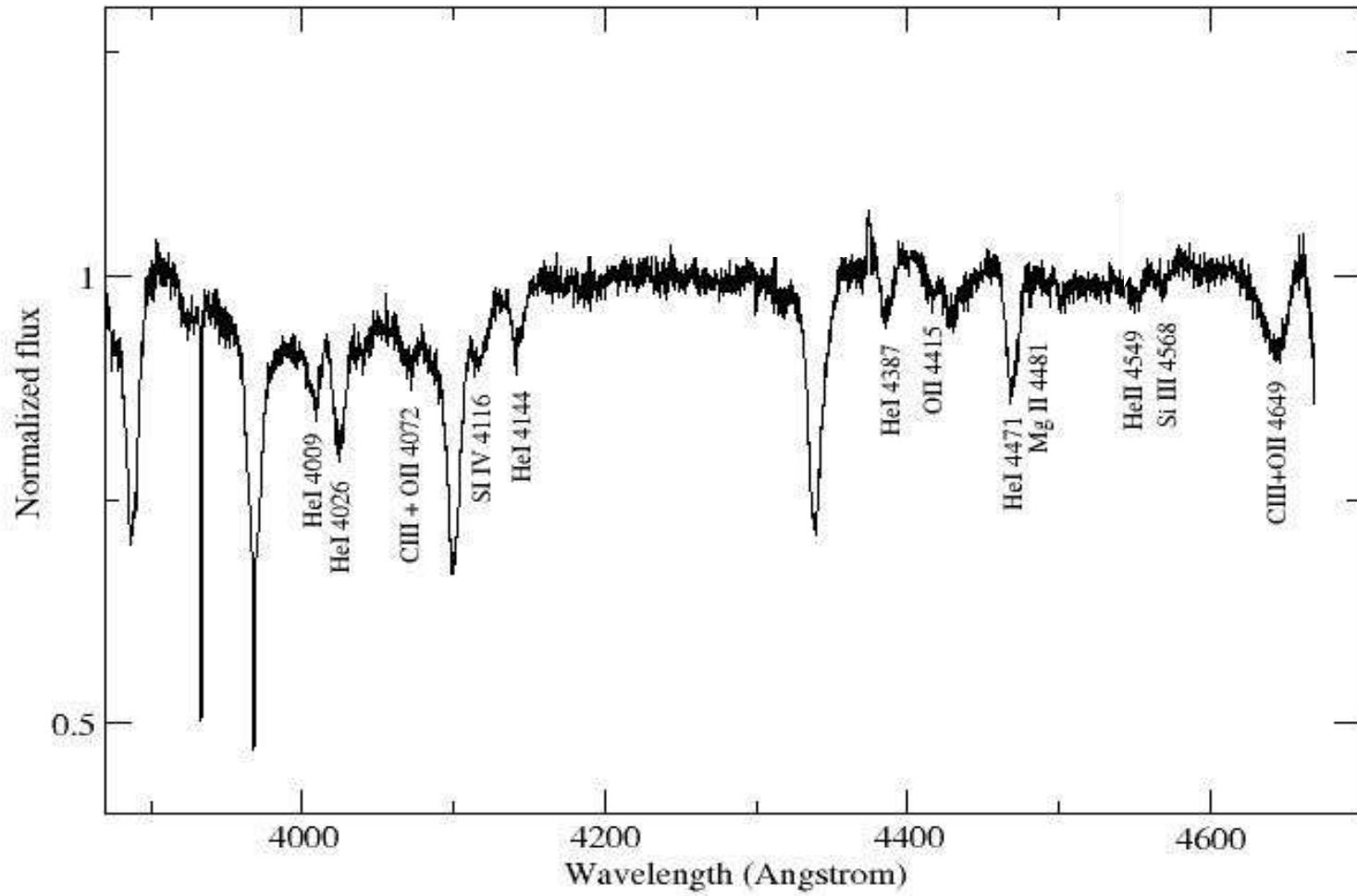
Figure 3.5: Spectral classification diagram.

Fig. 14—B0.2–B1.5 main sequence (the B0 V standard is in Figs. 3 and 23). The He I lines identified in HD 36959 are λλ4009,4026,4121,4144,4387,4471, and 4713. The spectral features identified in τ Sco are C III + O II λλ4070,4650 blends; Si IV λλ4089,4116; O II λλ4415–17, 4640; He II λλ4541,4686; and Si III λλ4552–68. The principal horizontal classification criterion in this spectral-type range is the ratio Si III λ4552/Si IV λ4089.

Figure 3.6: Template spectra by Walborn & Fitzpatric (1990)

The spectrum of the optical counterpart to IGR J21343+4738 is dominated by He I in adsorption indicating a hot blue-white B star. We can start by ruling out the most inappropriate spectral types. First of all, the classes O3-O9.5 can be rejected because strong HeII lines in the observed spectra do not exist. For the same reason, spectral type B0-B0.5 has been discarded. Mg II in absorption at 4481Å indicates a spectral type from B1-B3. However the strength of this line, can exclude the spectral types B2.5 and B3. Also the weakness of CIII+OII at 4649Å can confirm the above reasoning. The relative strength of SIII at 4649Å indicates a spectral type B1-B1.5. The existence and relative weakness of OII at 4415Å agrees with this classification. Moreover, giants and subgiants have been rejected because no NII line is present in the spectrum of IGR J21343+4738. Consequently, the spectral type of the optical counterpart to IGR J21343+4738 ranges from B1-B1.5 V and it is found in main sequence.

3.3   Determination of rotational velocity

The rotational velocity is a crucial parameter of Be stars and it remains a fundamental way to understand the formation of the equatorial disk. Generally, Be stars are fast rotators, it means that they have on average higher rotational velocity than B stars as a group. A rotational velocity close to the brake-up velocity reduces the effective equatorial gravity to the extend that weak processes such as gas pressure and/or non-radial pulsations may trigger the ejection of photosperic matter with sufficient energy and angular momentum to make it spin up into a Keplerian disc (Reig et al, 2010).

To estimate the rotational velocity of the optical counterpart to IGR J21343+4738 the methodology described by Steele et al. 1999 were used. By following this work, the rotational velocity was calculated by fitting Gaussian profiles on the HeI lines at 4026Å, 4143Å, 4387Å and 4471Å of the ''blue'' spectra. The width of these stellar absorption lines will give the estimated projected rotational velocity, vsini where v is the equatorial rotational velocity and i the inclination angle with respect of the line of sight. The equations created by the authors, are presented below.

$$vsini=41.25 \ F(4471) \ km \ s^{-1}$$
$$vsini=42.03 \ F(4387) \ km \ s^{-1}$$
$$vsini=44.51 \ F(4143) \ km \ s^{-1}$$
$$vsini=45.82 \ F(4026) \ km \ s^{-1}$$

where $F(\lambda)$ is the ful width at half maximum of the line with wavelength λ. The width of these lines was measured from the spectrum taken at 23-08-2013 because at this period no disk contribution was observed (Table 2.4). The final vsini is the mean of those derived from all the fitted lines and the error is the standard deviation. Because of the different definition of the continuum it was taken five different measurements for each line.

The results are presented in Table 3.3.

Table 3.3: Results of rotation velocity of each HeI line.

Wavelength	FWHM $_{corrected}$ (Å)	Vsini (km s^{-1})
4471 Å	8.81	403.90
	8.67	397.45
	8.77	402.14
	8.60	393.80
	8.58	392.94
4387 Å	8.40	384.93
	8.54	391.15
	8.50	389.54
	7.81	358.04
	8.07	369.70
4143 Å	8.51	389.81
	7.78	356.34
	8.44	386.91
	7.90	362.05
	8.01	366.84
4026 Å	7.48	342.73
	7.54	345.59
	6.84	313.38
	7.14	327.34
	7.25	332.06

The FWHM was measured by fitting Gaussian curves to the HeI absorption lines. The intrinsic value of FWHM of each line was calculated by subtracting in quadrature the width of the line due to the instruments:

$$\text{FWHM}_{corrected} = \sqrt{\text{FWHM}^2_{measured} - \text{FWHM}^2_{instruments}}$$

where FWHM$_{instruments}$ was measured approximately to be 0.8Å.

The average value of vsini is given by:

$$\overline{v\sin i} = \frac{\sum_{i}^{N} v\sin i_i}{N}$$

and the error is given by the standard deviation formula:

$$S_{\overline{v\sin i}} = \sqrt{\frac{\sum_{i}^{N} \left(\overline{v\sin i} - v\sin i_i\right)^2}{N-1}}$$

The resulting rotational velocity is:

$$\boxed{\text{vsini} = (370 \pm 27)\text{km s}^{-1}}$$

3.4   Determination of disk radius

The peak separation of the two Hα components is related to the size of the Be star's disk by (Huang 1972):

$$\frac{R_{disk}}{R*} = \left(\frac{2v\sin i}{\Delta_{peak}} \right)^2$$

where vsini is the projected rotational velocity of the B star (v the equatorial rotational velocity and i the inclination of the equatorial plane with respect to the observer) and R∗ is the star's radius. Using the results from the previous sections and the observations of Table 3.1, the disk radius was varying approximately from 1 R∗ to 3 R∗.

Chapter 4

Discussion

The objective of this project is to study the long-term optical properties of the optical counterpart to the X-ray source IGR J21343+4738 and the report of a disk-loss episode. It was found that this source is a Be star that went through a disk formation and dissipation episode.

4.1 Disk evolution

Figure 3.1 shows the evolution of the Hα line profile. The Hα line presents a formation-dissipation cycle. Hα in emission means existence of the disk and Hα in absorption indicates absence of disk. From 30-07-2009 until 06-09-2011 the line profile is in absorption therefore no disk exists around the star. Since 24-08-2012 until 04-01-2013 an emission line profile appears. This emission comes from an equatorial disk around the Be star i.e. the disk was performed during the period between 06-09-2011 and 24-08-2012. In the last observations the Hα line is noted in absorption and this means that the disk has disappeared in timescales of a few months. Also from figure 3.1 and Table 3.1 it is observed that the line became more asymmetric while the intensity was rising up. Moreover, at the beginning of the observations an increase of the strength of the Hα line exists. Also, the shape of the line changed from absorption dominated profile to emission line profile.

Figure 3.3 presents the equivalent width versus time diagram. The Hα EW represents a measure of the size of the disk. At 30-07-2009 the measurement of equivalent width showed a positive value therefore it presents an absorption line profile. From August 2011 until January 2013 the EW (Hα) showed negative values. Some months later, the observations indicated that the EW (Hα) became again positive, consequently the Hα line profile turned into absorption. In this point, a disk-loss episode is noted.

It is difficult to estimate the exact formation /dissipation cycle of the disk due to the incomplete observations. Many gaps in the available data exist so it is difficult to define the timescale for the formation/dissipation. Nevertheless, we can set a threshold of four years and this means that the formation/dissipation cycle of the disk is at least four years.

Figure 3.4 shows the peak separation diagram of the blue and the red peak in velocity units versus equivalent width. In is noted from the diagram that as the equivalent width increases, the peak separation, Δ_{peak}, decreases. It is known that the increase of the equivalent width means that the disk grows and so its radius R_e. Consequently, as the radius of the disk increases the velocity, Δ_{peak}, reduces.

This agrees with the Keplerian law of rotation, $V_{rot} \propto \dfrac{1}{\sqrt{R}}$.

By studying the V/R variability of the Hα line profile it is possible to obtain information about the structure of the equatorial disk. V/R is the cycle variation of the relative intensity of the blue (V) and red (R) peaks. V/R variability is believed to be caused by the gradual change of the amount of the emitting gas approaching the observer and that resending from the observer due to the procession of a density perturbation in the disk. Double-peak symmetric profiles are expected when the high-density part is behind or in front of the star, while asymmetric profiles are seen when the high density perturbation is on one side of the disk (Reig et al. 2010). When the high-density part of the disk is moving toward the observer, we expect to see a blue-dominated V>R line profile, while when the high-density part is removed from the observer, red-dominated profiles are expected. It was seen that V/R variability is appeared on time scales of months while the disk formation or dissipation appears on timescales of years.

In IGR J21343+4738 it is noted that as the disk grows, the Hα line changed from a symmetric to an asymmetric profile. Figure 3.2 presents the variability of the red and the blue peak versus time. V/R variability indicates the change of the shape of the Hα line profile. It is noted that the Hα line changed from a symmetric to an asymmetric profile. In the first observation, July 2009, log(V/R) is greater from the unit thus the blue peak is stronger than the red peak. Then, from autumn 2009 until autumn 2011 the Hα line changed from a symmetric to an asymmetric profile. From August 2012 to October 2012 the blue peak is dominated again (V>>R). Approximately, two months later the value of V/R ratio decreased very fast. This could mean that the V>R phase was ended.

4.2 Spectral Classification and contribution of the disk to the spectral lines

Spectral classification showed that the spectral type of the optical counterpart of IGR J21343+4738 ranges from B1-B1.5 V, in main sequence. This conclusion agrees with the fact that most Be X-ray Binaries are main sequence stars in B0-B3 spectral type.

Figure 4.1 shows a comparison of a region of two blue spectra of IGR J21343+4738 taken from WHT at two different epochs. At 26 December 2012 the spectrum corresponds to a Be phase when the Hα line was in emission (black line), while on 23 August 2013 the spectrum corresponds to a B phase when this line has an absorption profile (red line). From the visual comparison it is clear that when the disk is present, the width of spectral lines (especially those of Balmer series and He I lines) is significantly narrower when the disk is present. It means that the rotational velocity of the star must be measured when the disk dissapears.
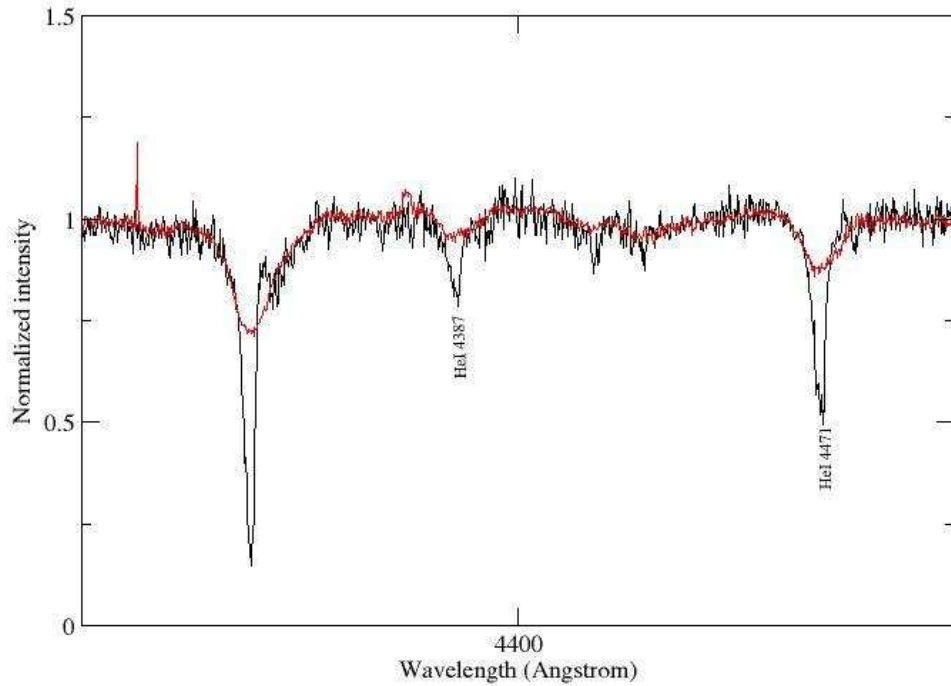
Figure 4.1: Comparison of two spetra of IGR J21343+4738 at different epochs, when the disk was present (black line) and when the disk has disappeared (red line). The spectra were taken from WHT on 26 December 2012 and on 23 August 2013.

4.3 Rotational velocity

A crucial characteristic of Be stars is that they are rapidly rotating B-type stars that lose mass in an equatorial circumstellar disk. An existing hypothesis is that the rotational velocity of the Be star may is the cause of the existence of the decretion disk. This velocity is called critical velocity and it defined as the velocity at which centrifugal forces balance Newtonian gravity at the equator. For a centrally condensed star, the critical velocity is given by:

$$u_c = \sqrt{\frac{GM_*}{R_e}}$$

where the ''e'' refers to the equatorial value.

For a star of spectral type B1-B1.5 the critical velocity is expected to be about 500 km s^{-1} (Townsend et al. 2004). The value of the rotational velocity of IGR J21343+4738 is estimated at 370 km s^{-1}. This value of rotational velocity is about $\frac{2}{3}$ of the critical value (assuming that i~90°⇔sini=1 due to the shell profiles observed (Porter & Rivinius 2003)). Also, it is possible to compare this result with Figure 4.2 below assuming that the B type stars have approximately a mass of 10 solar masses. So, the resulting rotational velocity of B type stars is approximately 270 km s^{-1} less than the rotational velocity of the optical counterpart of IGR J21343+4738. This result agrees with the fact that Be stars are fast rotators and they rotate with rotational velocities greater that B type stars. Consequently the high rotational velocity of the optical counterpart of IGR J21343+4738 could be the main mechanism that expels matter from the photosphere to create the disk.
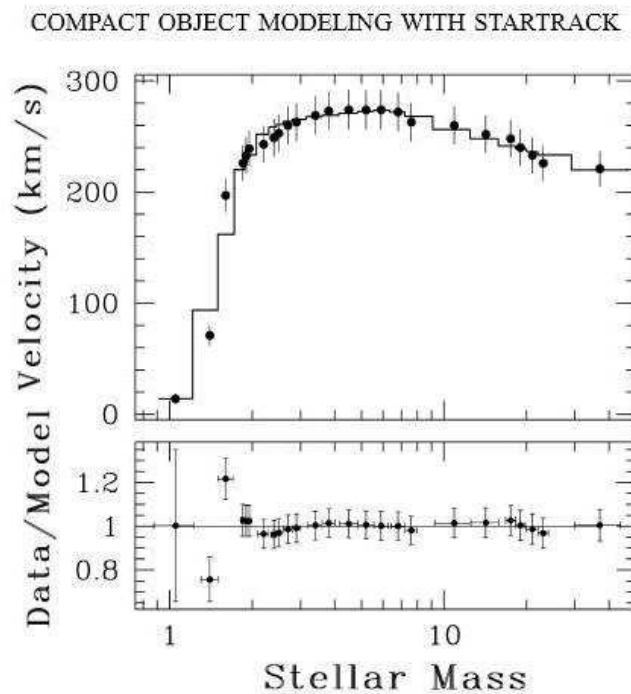

Figure 4.2: Velosity versus stellar mas diagram (Belczynski et al. *2008)*

4.4 Comparison of IGR J21343+4738 with other Be/X-ray binaries

Based on the work of P. Reig et al (2010), a comparison of IGR J21343+4738 with other Be/X-ray binaries is presented (Table 3.4).

Table 3.4: Comparizon of IGR J21343+4738 with other Be/X-ray binaries

X-Ray source	Optical counterpart	Spectral type	Disk-loss episode	Vsini (km s^{-1})
IGR J21343+4738	-	B1-1.5V	yes	370±27
IGR J06074+2205	-	B0.5IV	yes	260±20
4U 0115+634	V635 Cas	B0.2V	yes	300±50
RX J0146.9+6121	LSI +61 235	B1III-V	no	200±30
V 0332+53	BQ Cam	O8-9V	no	<150
X-Per	HD 24534	O9.5III	yes	215±10
RX J0440.9+4431	LS V +44 17	B1III-V	yes	235±15
1A 0535+262	HD 245770	O9.7III	yes	225±10
RX J0812.4-3114	LS 992	B0.5III-V	yes	240±20
1A 1118-615	Hen 3-640	O9.5IV	no	300
4U 1145-619	V801 Cen	B0.2III	no	250±30
SAX J2103.5+4545	-	B0V	yes	240±20

Columns 1&2 give the name of the X-ray source and the name of the optical counterpart respectively, where exists. Column 3 shows the spectral type according to the spectral classification carried out for each optical counterpart. Column 4 indicates the existence or not of a disk-loss episode and the last column gives the projected rotational velocity of each optical counterpart. Comparing IGR J21343+4738 with the other Be X-ray Binaries it is noted that IGR J21343+4738 has the greater velocity as well as later spectral type from the other stars.

Chapter 5

Conclusion

The aim of this project was to analyze optical spectroscopic observations of the optical counterpart to the X-ray source IGR J21343+4738. The observations showed that IGR J21343+4738 is a high-mass X-ray binary with a Be companion and also a disk-loss phenomenon is reported. By its long-term optical spectroscopic variability many changes in the structure of the equatorial disk were noticed. Changes in the structure of the Hα line declared the formation and dissipation status of the disk. It was found that the entire formation/dissipation cycle is at least 4 years.

From the absence of the disk, it was able to determine the physical characteristics of the Be star. The estimation of the rotational velocity showed that the rotation of the Be star is the main mechanism that expels matter from the photosphere to create the disk. Also, the comparison of the ''blue'' spectral lines with of existence and absence of the disk revealed that when the disk is present, the width of spectral lines (especially those of Balmer series and He I lines) is significantly narrower.

References

P. Reig, *Be/X-ray binaries* (Invited Review): Astrophysics Space Science, **332**, 1-29 (2011)

P. Reig, A.Zezas, L. Gouvelis, *The optical counterpart to IGR J06074+2205: a Be/X-ray binary showing disc loss and V/R variability*: A&A, **522**, A107 (2010)

Nolan R. Walborn, Edward L. Fitzpatrick, *Contemporary optical spectral classification of the OB stars: a digital atlas*: Publication of the Astronomical society of the pacific, **102**, 379-411 (1990)

John M. Porter, T. Rivinius, *Classical Be stars* (Review): Publication of the Astronomical society of the pacific, **115**, 1153-1170 (2003)

J. Ziolkowski, *Be X-ray Binaries*: Memorie della Societa Astronomica Italiana, **73,** 1038-1038 (2002)

P. Reig, A. Slowikowska, A. Zezas, P. Blay, *Correlated optical/X-ray variability in the high-mass X-ray binary SAX J2103.5+4545*: Monthly Notices of the Royal Astronomical Society, **401**, 55-66 (2010)

K. Belczynski, V. Kalogera, F. A. Rasio, R. E. Taam, A. Zezas, T. Bulic, T. J. Maccarone, N. Ivanova, *Compact object modeling with the startrack population synthesis code:* The astrophysical Journal supplements series, **174**, 223-260 (2008)

R. H. D. Townsend, S. P. Owocki, I. D. Howarth, B*e-star rotation: how close to critical?* : Monthly Notices of the Royal Astronomical Society, **350**, 189-195 (2004)

 I. A. Steele, I. Negueruela, J. S. Clark, *A representative sample of Be stars*: Astronomy and Astrophysics supplement series, **137,** 147-156 (1999)

J. Silaj, C.E. Jones, C. Tycner, T.A.A. Sigut, A.D. Smith, *A systematic study of Ha profiles of Be stars* :The Astrophysicsl Journal, **187**, 228-250 (2010)

P. Reig, R. Roche, *Discovery of two new persistent Be/X-ray pulsar systems*: Monthly Notices of the Royal Astronomical Society, **306**, 100-106 (1999)

J. Frank, A. King, D. Raine, *Acretion Power in Astrophysics*, Cambridge University Press (2002)

M. Seeds, D. Backman, *Foundations of astronomy*, Brooks/Cole (2012)

F. Seward, Ph. Charles, *Exploring the X-ray universe,* Cambridge (2010)

O. G. Richard, C. J. Corbally, *Stellar spectra classification,* Princeton series Astrophysics (2009)

B. W. Carroll, D. A. Ostlie, *An introduction to modern astrophysics*, Pearson Addison-Wesley (2007)

Appendix A

Equivalent width

The equivalent width of W of a spectral line, is defined as the width of a box reaching up to the continuum that has the same area as the spectral line. That is,

$$W = \int \frac{F_c - F_\lambda}{F_c} \, d\lambda$$

where the integral is taken from one side of the line to the other. Another measure of the width of a spectral line is the change in wavelength from one side of the line to the other, where its depth $(F_c-F_\lambda)/(F_c-F_{\lambda o})=1/2$; this is called the *full width at half maximum*.

Figure below shows a graph of the radiant flux, F_λ, as a function of wavelength for a typical absorption line. In the figure, F_λ is expressed as a fraction of F_c, the value of the flux from the continuous spectrum outside the spectral line. Near the central wavelength, λ_o, is the *core* of the line, and the sides sweeping upward to the continuum are the line's *wings*.
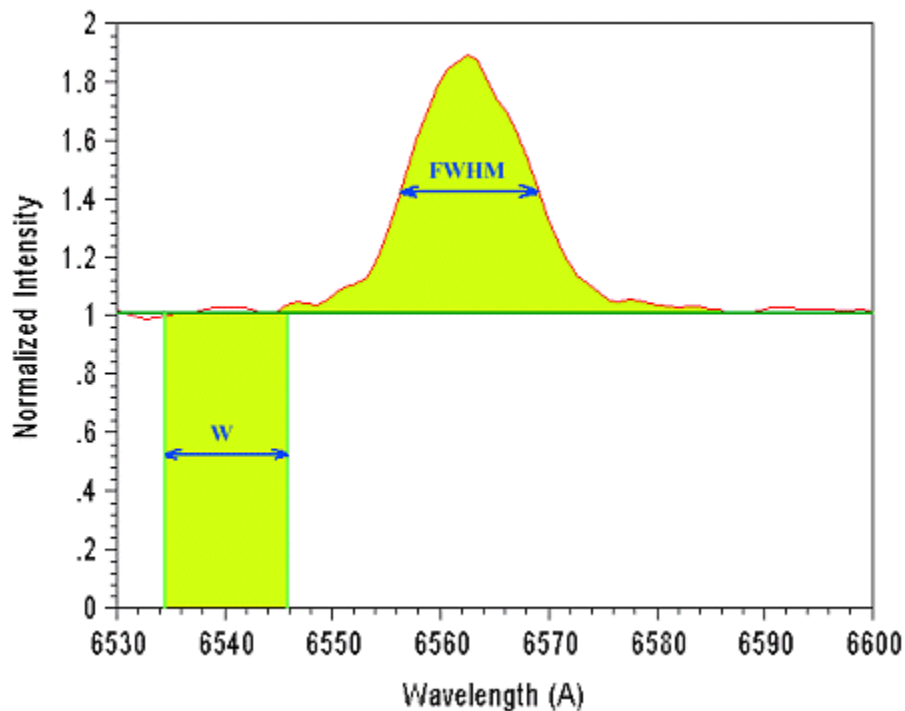

Figure A: Equivalent width and Full width at half maximum.
(http://www.astrosurf.com/buil/us/spe2/hresol7.htm)